Transport of physisorbed Xe atoms on Ni(110) using a scanning tunneling microscope: A theoretical approach

J.R. Cerdá and P.L. de Andres
Instituto de Ciencia de Materiales, Consejo Superior de Investigaciones Científicas, Serrano 144, E-28006 Madrid, Spain

F. Flores and R. Perez
Departamento de Fisica de la Materia Condensada, Universidad Autónoma de Madrid, Cantoblanco, E-28049 Madrid, Spain
(Received 8 October 1991)

Using a simple theoretical model we have simulated the conditions under which a scanning tunneling microscope is able to transport a physisorbed xenon atom sitting on a nickel (110) surface. Simple calculations of the tunnel current for the atomic geometries derived using the former model are in good agreement with an elegant experiment performed by Eigler and Schweizer on the same system [Nature **344**, 524 (1990)]. On these theoretical grounds, we discuss in detail how different conditions affect the transport process for this system.

I. INTRODUCTION

In a recent work, Eigler and Schweizer[1] have reported an interesting experiment where xenon single atoms physisorbed on a Ni(100) surface were positioned with atomic precision at will using a scanning tunneling microscope (STM). The experiment was performed at low temperature (4 K), thus avoiding any thermal diffusion of the physisorbed species on the substrate and ensuring that the process is, in principle, temperature independent.

Moving a single Xe atom along the surface was carried out basically as a three-step process: (i) First, a scanning of the surface was done in order to locate the Xe atoms originally physisorbed. After locating one of those atoms, the tip is stopped right above this site and then lowered until sufficient attractive force between the tip and the atom is achieved. At this moment, (ii) the tip is moved slowly across the surface under closed-loop conditions, dragging the Xe atom with it, until the desired new location is reached. Then, (iii) the tip was raised reducing its interaction with the Xe, leaving the atom underneath on the new desired physisorbed site. The fact that the magnitude or sign of the applied voltage had no appreciable effect in the whole process is a clear indication that the system could be, in principle, studied neglecting any tunneling current (as far as the transport is concerned), regarding it merely as an accurate tool to establish the tip sample distance.

As the importance of this experiment is clear from the possible implications to the design of quantum devices, we have performed a theoretical study of the process, trying to understand a number of questions, such as whether the tip is pushing or pulling the atom, whether a simple van der Waals model would be able to explain the experiment and under which conditions (shape and height of the tip, influence of possible contaminants, etc.) will the transport occur. A general good agreement between our theoretical model and the description given by Eigler and Schweizer is found and we have been able to show that values for tunneling currents during the dragging process used by these authors are in accordance with the values we obtain using a simple model for the tunneling process,[2,3] when considering the geometrical limits we derive on the positions of the tip and the Xe atom with respect to the Ni surface.

Further evidence for the controlled movement of atoms with the STM, but using voltage pulses to transfer atoms from the tip to the substrate and vice versa, have been reported,[4–6] including a wide variety of chemical species.

II. THE TUNNELING CURRENT

In Fig. 1 we show the four tips that have been considered in our analysis. The tips are grown according with the parameters that correspond to a tungsten bcc crystal along the ⟨110⟩ and ⟨111⟩ directions. In all cases the growth is in a pyramidal form with a rhombic base for the (110) plane and a triangular one for the (111) case. No relaxations or reconstructions have been considered, with the atoms keeping their bulk distances. This particular choice was based on the two following reasons: (i) It is known that the standard way of creating W tips produces most likely atomic orientations along the (110) plane[7] and (ii) a sharp tip is expected to be obtained at the "corners" where different (110) planes meet, with the structure of these corners resembling a (111) plane. To test different sharpnesses, in each case the tip was allowed to end up either in just one atom (sharp tips) or in the lowest platform possible: a rhombic four-atom base for the (110) case, or a three-atom equilateral triangle for the (111) (flat tips).

In this section we discuss how to calculate the tip-sample tunneling current in two different cases: (i) for a clean Ni(110) surface and (ii) for a xenon atom physisorbed on the nickel surface. For the moment the surface geometry is assumed to be known. In the next section we shall discuss how to calculate the xenon equilibrium site on the Ni(110) surface as a function of the tip position. Figure 2 shows the interface geometry of the tunnel-

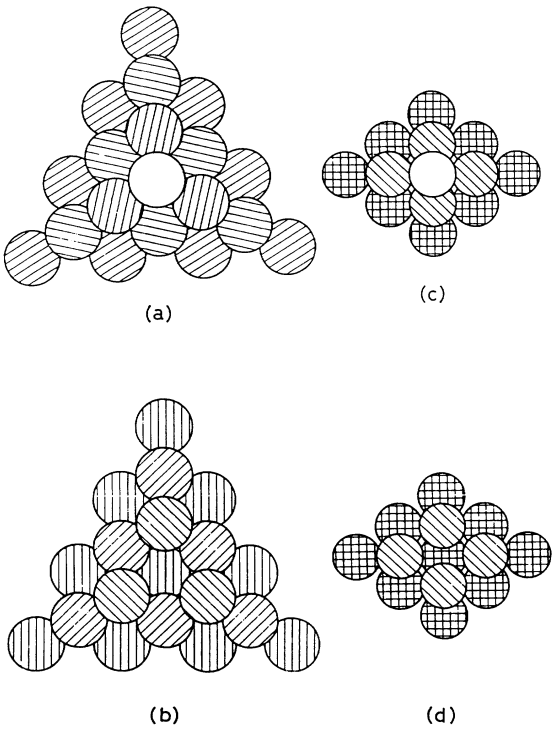

FIG. 1. Simulated STM tips studied in this work; (a) sharp (111); (b) flat (111); (c) sharp (110); and (d) flat (110).

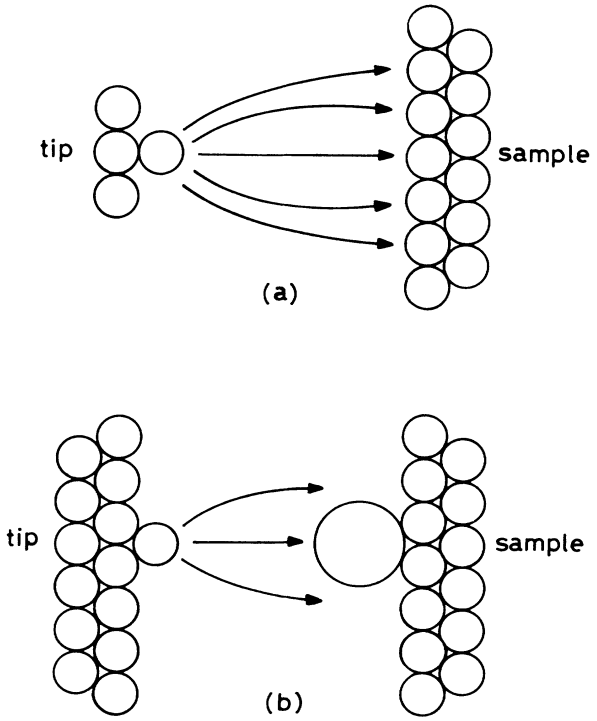

FIG. 2. Interface geometry for (a) a W tip and a metal surface, and (b) the same system with a Xe atom physisorbed at the surface.

ing problem we consider in this section. In our analysis we follow the tight-binding prescription as discussed in Refs. 2 and 3. In this approach the tunneling current is calculated by means of the hopping interactions T_{kl} appearing between the different orbitals of the tip and the sample. First, consider case (a) of Fig. 2. As an initial step, we assume that the tunneling current only flows from a single tip atom to another single substrate atom. This interface is then defined by the following Hamiltonian:

$$H = H_{\text{tip}} + H_{\text{sample}} + H_{\text{int}}, \tag{1}$$

where H_{tip} and H_{sample} refer to the tip and the sample atoms, respectively, and

$$H_{\text{int}} = \sum_{k,l,\sigma} T_{kl}(c^{\dagger}_{k,\sigma} c_{l,\sigma} + c^{\dagger}_{l,\sigma} c_{k,\sigma}), \tag{2}$$

where k and l refer to the atomic orbitals associated with the tip and the sample atoms, respectively. The tunneling current I across the interface can be obtained by way of the Keldysh method[8] as applied in Ref. 9. In Ref. 3, it has been shown that the tunneling current I for a small bias V is given by the following equation:

$$I = \frac{4e^2 V}{\pi\hbar} \frac{x}{(1+x)^2}, \tag{3}$$

where

$$x = \pi^2 \sum_{k,l} |\, T_{kl} \,|^2 \, \rho^{(0)}_{kk}(E_f) \rho^{(0)}_{ll}(E_f), \tag{4}$$

where $\rho^{(0)}_{kk}(E_F)$ and $\rho^{(0)}_{ll}(E_F)$ are the density of states at the Fermi level, associated with the orbitals k and l of the tip and the sample atoms. Equation (3) is still valid for very small tip-sample distances, as all higher-order terms in the hopping parameter T_{kl} are included in the denominator, so that the resistance saturates (when $x \approx 1$) at close contact, its value being $h/2e^2$. In our calculation we have only considered the contribution to the tunneling current due to the conduction s bands of W and Ni, since the corresponding d bands are too localized. As for $\rho^{(0)}_{kk}(E_F)$ and $\rho^{(0)}_{ll}(E_F)$, the bulk density of states for the s bands, $\rho^{s}_{E_F}(Ni)$ and $\rho^{s}_{E_F}(W)$, were used;[10] small changes in these values due to the surface effects are negligible compared with the most important contribution due to the coupling T_{kl}. This hopping interaction, T_{kl}, between the tip and sample orbitals is calculated using the following equations:

$$T_{kl} = \gamma_{AB} T^{B}_{kl} T^{B}_{kl} = \frac{\hbar^2}{2m} \int_{\sigma_{kl}} [\psi^{*}_{k} \nabla \psi_l - \psi^{*}_{l} \nabla \psi_k] \cdot d\mathbf{S}, \tag{5}$$

where σ_{kl} is a surface between the orbitals k and l, chosen such that the following condition is satisfied:

$$\tfrac{1}{2} \int_{\Omega} \psi_k \psi_l d\mathbf{r} = \int_{\Omega_k} \psi_k \psi_l = \int_{\Omega_l} \psi_k \psi_l, \tag{6}$$

where the whole space is split into the subspaces Ω_k and

Ω_l by the surface σ_{kl}: $\Omega = \Omega_k + \Omega_l$.

For Ni, we use the $4s$ orbital given by Clementi and Roetti[11] and for W we have taken the tabulated wave functions of Herman and Skillmann.[12] Furthermore, in Eq. (5) γ_{AB} is a parameter close to 1.5,[13] which takes into account the long-range order of the atomic potentials.

Finally, as Eq. (3) has been deduced for just one single tip atom and another single substrate atom, we must generalize this expression in order to take into account all other substrate and tip atoms. Within our tight-binding approach, and neglecting any interference between adjacent atoms, this generalization yields

$$I = \frac{4e^2V}{\pi\hbar} \sum_j \frac{x_j}{(1+x_j)^2}, \tag{7}$$

where j refers to the tip atoms and x_j is now given by

$$x_j = \pi^2 \sum_i |\, T_{ij} \,|^2 \rho^s_{E_F}(Ni) \rho^s_{E_F}(W), \tag{8}$$

the label i indexing the sample atoms.

Let us now turn our attention to case (b) of Fig. 2, with the xenon physisorbed on Ni. The new contribution to the current appearing in this case is associated with the electrons tunneling between the tip and the sample through the xenon orbitals. We have found that the most important contribution to this tunneling current is due to the first empty orbital of xenon, the $6s$ level, in good agreement with the results of Eigler *et al.*[14] Here, we discuss how to obtain the Xe tunneling current by including only this interaction between this $6s$ level and the s levels of W and Ni. In general, we follow the same procedure discussed above; there is, however, a difference: for xenon, the interactions $T_{\mathrm{Xe},i}$ and $T_{\mathrm{Xe},j}$ with the tip and the sample never become too large, as the Xe $6s$ wave function, although very extended, presents a rather small main peak when compared to other filled orbitals. Then, the tunneling current can be calculated up to second order in $T_{\mathrm{Xe},i}$ and $T_{\mathrm{Xe},j}$. Following the discussion of Ref. 2, we have obtained for the tunneling current through the Xe,

$$I_{\mathrm{Xe}} = \frac{4e^2V}{\pi\hbar} \sum_j x_j, \tag{9}$$

where

$$x_j = \pi |\, T_{\mathrm{Xe},j} \,|^2 \sum_i |\, T_{\mathrm{Xe},i} \,|^2 \rho^s_{E_F}(\mathrm{Ni}) \rho^s_{E_F}(W) \times |\, G_{\mathrm{Xe}}(E_F) \,|^2, \tag{10}$$

$G_{\mathrm{Xe}}(E_F)$ being the Green function associated with the xenon $6s$ orbital at the Fermi energy. A good approximation to $G_{Xe}(E_F)$ is to take

$$G_{\mathrm{Xe}} = \frac{1}{E_f^{(\mathrm{Ni})} - E_{\mathrm{Xe}}(6s)}, \tag{11}$$

where $E_{\mathrm{Xe}}(6s)$ is the 6s atomic level of Xe. For this case, we have used an atomic local-density-approximation (LDA) calculation,[15–17] obtaining the $6s$ wave function and its energy level that appears to be located 0.53 eV below the vacuum level. For the Ni energy at the Fermi level, $E_F^{(\mathrm{Ni})}$, we have taken the experimental value given in Ref. 18. The different hopping terms between xenon and the metals were calculated by using Eq. (5) and the corresponding atomic wave functions.

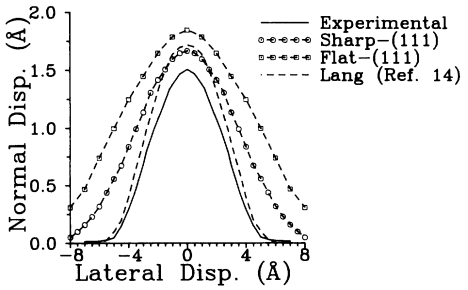

FIG. 3. Normal tip displacement (Å) vs the lateral tip displacement (Å) when scanning the Xe atom at a constant tunneling current of 1×10^{-9} A [only (111) tips are shown for clarity].

Equations (7) and (9) are the main theoretical formulas that allow us to calculate the tunneling current between the tip (Fig. 1) and the ideal Ni(110) sample, with and without a xenon atom physisorbed on the surface. We have concluded that this approach affords a reasonable way of calculating tunneling currents, by analyzing the perpendicular displacement of the tip as a function of the relative sample-tip position for xenon physisorbed on nickel, keeping constant the total intensity. This intensity is normalized to the experimental one used by Eigler *et al.* to observe the xenon atom physisorbed on the nickel (110) surface (1×10^{-9} A). Figure 3 shows our results for the (111) tips, comparing them with the experimental evidence and the theoretical results obtained by Eigler *et al.* following Lang's approach.[14] It should be noticed that the two (110) tips yield protrusions very similar to the sharp (111) one, and are not shown in the figure for the sake of clarity. One then finds a reasonable agreement in all cases, except for the flat (111) tip, where both a too high normal displacement and a too broad signal appears (thus this tip could in principle be discarded, although it has actually been included in the calculations following this section). The rest of the tips also gave a slightly broader signal when compared to experiment; an effect which we believe to be related to the LDA calculation of the xenon $6s$ orbital. Nevertheless, Fig. 3 indicates that our simple procedure is good enough to calculate the different tunneling currents associated with the actual tip-adsorbate-sample geometry.

III. THE INTERACTION OF XENON WITH THE METAL SURFACE

Systems involving noble gases physisorbed on metal surfaces have been the object of a variety of theoretical and experimental studies.[19] In general, the interaction of noble gases and metal surfaces can be understood in the following terms: (i) at long distances, the neutral atom

TABLE I. Quantities used in the Lennard-Jones parametrization. Energies are experimental values, while the van der Waals coefficients are semiempirical ones.

	Xe-W	Reference	Xe-Ni	Reference
Heat of adsorption (meV)	395	26	220–280	27,28
C_3 (meV Å^3)	3591	24	3056	24

is attracted by the surface due to electron correlation effects that are well described by Lifschitz's formula, which yields an interaction going like $-C_3/z^3$, with z being the distance between the atom and the surface and C_3 a coefficient depending on the metal dielectric function and the adatom polarizability, (ii) at short distances a repulsive interaction appears mainly due to the increase in the electron kinetic energy of the system, arising from the overlap between the electron clouds of the metal and the adatom.

The description of the metal adatom interaction has been fully analyzed by many different authors.[20,13,21] In the He case, the short-distance interaction has been shown to be well described by using a local interaction such that a repulsive potential is proportional to the local metal density:

$$V_{\text{repulsive}}(\mathbf{r}) = \alpha n_{\text{metal}}(\mathbf{r}), \tag{12}$$

where α is a constant depending on the metal and the adatom properties. As the surface metal density can be well described as the superposition of the densities associated with each metal atom, Eq. (12) takes the form

$$V_{\text{repulsive}}(\mathbf{r}) = \alpha \sum_i n_{\text{i,metal}}(\mathbf{r}), \tag{13}$$

where n_i describes the electron density of atom i. Equation (13) shows that the total repulsive energy between He and the metal can be written as the linear superposition of the different repulsive energies between He and each metal atom. This analysis is closely related to the embedded-atom model that assumes an atom-metal interaction to be basically described by an equation similar to Eq. (12) given above. We shall assume that the same equations [either (12) or (13)] are satisfied by the xenon-metal interaction.

On the other hand, the long-range interaction between xenon and the metal has also been analyzed by many authors.[20,22–24] As mentioned above, this interaction goes like $-C_3/z^3$. The important point to notice here is that this interaction can be obtained as the linear superposition of the long-range van der Waals interaction, $-C_6/z^6$, operating between two neutral atoms:[25]

$$-C_3/z^3 = -\sum_i \frac{C_6}{r_i^6}, \tag{14}$$

where i refers to a metal atom, r_i is the distance between the xenon and the atom i, and C_6 is a constant that can be fitted to yield Eq. (14).

Equations (13) and (14) show that the metal-xenon interaction can be described as the superposition of the different potentials, $V_i(r)$ given by

$$V_i(r) = \alpha n_{i,\text{metal}}(r) - C_6/r_i^6 \tag{15}$$

with αn_i describing the repulsive part of the metal-xenon interaction and $-C_6/r^6$ its attractive long-range part.

In our approach to the analysis of the metal-xenon interaction, we propose to replace Eq. (15) by the more conventional Lennard-Jones potential:

$$V_i(r) = 4\epsilon(\sigma/r_i)^{12} - (\sigma/r_i)^6, \tag{16}$$

where the repulsive term $4\epsilon(\sigma/r)^{12}$ represents a standard approximation to $\alpha n_i(r)$. Equation (16) depends on two parameters, ϵ and σ. Instead of attempting a first-principles calculation of them, we have chosen to fit them to two independent quantities: the heat of adsorption of xenon on the metal, and the van der Waals long-range interaction given by $(-C_3/z^3)$. A good fit to these quantities (see Table I) is obtained with the parameters of Table II. We should stress that the parameters given in table II for σ are slightly smaller (around 10%) than the usual sum of the Pauling radii for Xe and the corresponding metal atom. This reduction in σ allows us to get a good fitting in the two data mentioned above, the heat of adsorption and the van der Waals interaction.

TABLE II. Parameters fitting the Lennard-Jones potential to the quantities of Table I. Energies are reproduced within 1 meV accuracy, while the van der Waals coefficients yield a 30% overstimation.

	Xe-W	Xe-Ni
σ (Å)	3.0	3.0
ϵ (meV)	46.7	27.4

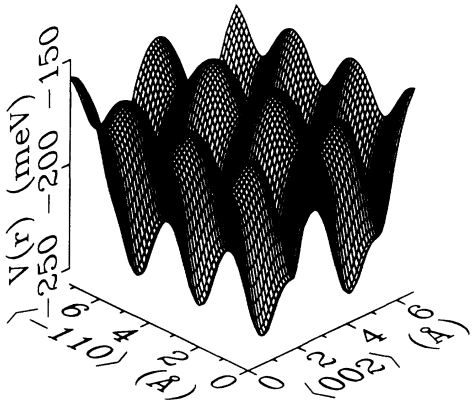

FIG. 4. Potential energy surface obtained when minimizing the Lennard-Jones interaction between the Ni substrate atoms and the Xe adsorbed atom with respect to the Xe [110] coordinate.

Using the values given in Table II, we have calculated the potential-energy profile of the xenon atom physisorbed on a Ni(110) surface. We display this potential in Fig. 4 for a grid made of three surface unit cells in the [$\bar{1}$10] direction (x) and by two unit cells in the [002] direction (y). For each point on this grid, the potential given by Eq. (16) (summing up all the metal atoms) was minimized with respect to z to yield the surface displayed in the figure. In Table III we give the xenon binding energies to the nickel surface at four different typical adsorption sites.

It is clear from these results that the xenon transport will be easier through the [$\bar{1}$10] direction than along the [002] one, as the corrugation is smaller in this case. This is in accordance with the results of Eigler and Schweizer.

In simulating the experiment by Eigler and Schweizer, the xenon atom was initially left at the fourfold site, and the center of the tip was placed on top of the Xe atom. The tip was then successively moved along the [$\bar{1}$10] direction keeping the other coplanar coordinate (the [002]) fixed for a given tip height (we define the tip height as the normal distance from a Ni top atom at the surface to the tip end atom or platform). The potential energy in this situation is calculated adding the interaction of the Xe atom with the nickel and tungsten as independent:

$$V(r, r^*) = V_{\text{Xe-Ni}}(r) + V_{\text{Xe-W}}(r^*), \tag{17}$$

where r^* denotes the distance from the xenon to the tungsten atoms, r its distance to the nickel ones, and V takes the functional form given in Eq. (16). Using this simple expression the potential was minimized for every fixed tip coordinate r^* with respect to the normal coordinate z, throughout three entire consecutive surface unit cells. By following the evolution of the potential minimum as the tip was moved step by step, it was determined whether the Xe transport was successful or not. The same scheme was then used for the [002] direction.

The tip height was kept constant throughout the carriage, this not being the exact experimental situation, as Eigler-Schweizer transport was performed at constant tunneling current. However, we have tested the influence of this correction to find that it is negligible in all cases. To perform the summation in the Lennard-Jones expression for nickel we have considered a 50 × 50 × 50 region of material along the three bulk unit cell directions. This was tested for convergence against a 100 × 100 × 100 case to find that differences were smaller than 1 meV. For the tungsten tip, the summation was performed vertically up to 40 layers, taking for each layer all the tungsten atoms present according to the pyramidal growth. The minimization respect to z was made with a numerical error of ±0.005 Å.

TABLE III. Xenon binding energies to the Ni surface for four typical surface sites. Energies are taken from Fig. 4 and the adsorption heights are given with respect to a Ni top atom.

Surface site	Binding energy (meV)	Adsorption height (Å)
Center	260	2.41
Top	157	3.10
Short bridge	178	2.95
Long bridge	226	2.60

IV. DISCUSSION FOR THE TRANSPORT

The four tips considered were found to carry the xenon physisorbed atoms, but yielding different geometrical constraints. Below we shall explain in detail the transport procedure for the cases analyzed, only considering the [002] direction (y), which represents the most difficult case for the carriage.

Let us first consider the (111) sharp tip. In Figs. 5(a), 6(a), and 7(a) we have plotted the xenon y coordinate obtained after the minimization explained above, as a function of the tip y coordinate for three different tip heights: z_{tip} =4.0, 4.8, and 5.6 Å. One finds that for each tip position, the xenon atom is never located directly below the center of the tip, but always a few angstroms behind, as can be seen in Figs. 5(b), 6(b), and 7(b), where the transport's atomic geometry is depicted. This implies that the very end of the tip does not exert enough force on the xenon atom as to surpass the surface corrugation, so that tip sites providing a greater number of nearest neighbors (these are high coordination points at the slopes) are responsible for the carriage process, or in other words, they give the main contribution to the attractive van der Waals forces. As expected, the smaller

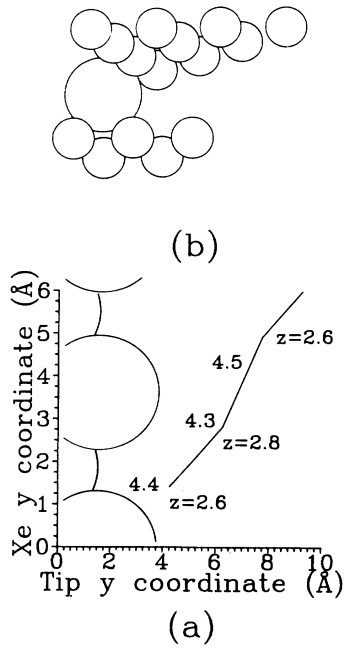

FIG. 5. Description of the transport for the sharp (111) tip at a tip height of z_{tip} = 4.0 Å. (a) The graph shows how the Xe atom moves across the surface along the [002] direction (y axis) as the tip is displaced (x axis), and (b) relative tip-adsorbate-substrate positions at an instant of the transport where the Xe is at the hollow site; the Pauling radii have been used to determine the atomic sizes in the figure.

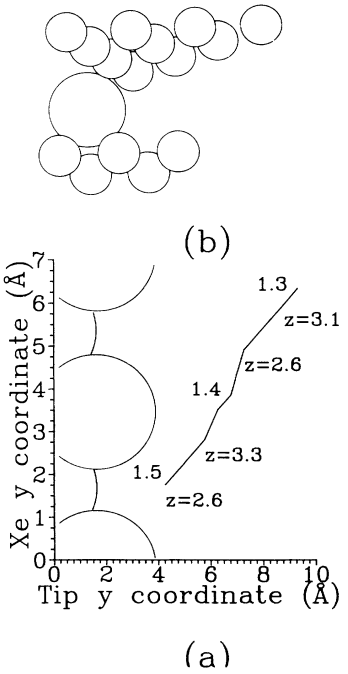

FIG. 6. Same as Fig. 5, but for a tip height of $z_{tip} = 4.8$ Å.

the tip height, the lateral separation between the xenon atom and the tip midpoint (hereafter called y distance) becomes progressively greater (for instance, at $z_{tip} = 4.0$ Å this lateral distance is around 3.1 Å, while for $z_{tip} = 5.6$ Å, this value diminishes to around 2.2 Å).

It should also be noticed that, for a fixed tip height, the y distance does not keep a constant value throughout the carriage, so that when pulling the noble atom from the fourfold site to the bridge site, this value attains a maximum. At this point, the y distance starts diminishing [as can be seen from the increase in the slope in Figs. 5(a), 6(a), and 7(a)] and the xenon atom "precipitates" to the new fourfold site at the next surface unit cell. This stepped process is then again repeated as the tip is moved further, so that one can regard this transport as a hopping process. This hopping effect is enhanced as the tip height increases, as a consequence of the decrease in the xenon-tip interaction; this becomes clear at $z_{tip} = 5.6$ Å—see Fig. 7(a).

In Figs. 5(a), 6(a), and 7(a) numbers on the left of data points give the tunneling current ($\times 10^{-8}$ A) estimated according to the formulas discussed in Sec. II, considering the tunneling both through the xenon atom and directly from metal to metal. The intensity values remain fairly constant (within 15%) for each tip height, thus confirming that the approximation of keeping the tip height constant is a good procedure.

When comparing these tunneling currents with those reported by Eigler and Schweizer [$(1-6) \times 10^{-8}$ A], one finds an excellent agreement for tip heights ranging from 3.9 to 5.0 Å. For greater tip heights, the hopping terms W-Ni become negligible, and the main contribution to the tunnel current is that going through the xenon atom, which in turn, and as mentioned in Sec. II, cannot attain too high intensities (around 0.8×10^{-8} A).

A final important feature arises from the fact that about 3 Å to the left of the tip midpoint (along the [002] direction), and in the absence of the metal surface, the tip slope would physisorb the xenon atom with a binding energy of at least 280 meV (thus always greater than that at the nickel surface hollow site; see Table III). This can be seen from Fig. 8, where we display the sharp (111) tip energy profile as seen by a xenon atom in the absence of the nickel surface. Since these binding energies correspond to normal distances from the xenon to the tip edge of around 1 Å, it would be expected that if the tip slope could come closer to the xenon atom (closer than 1

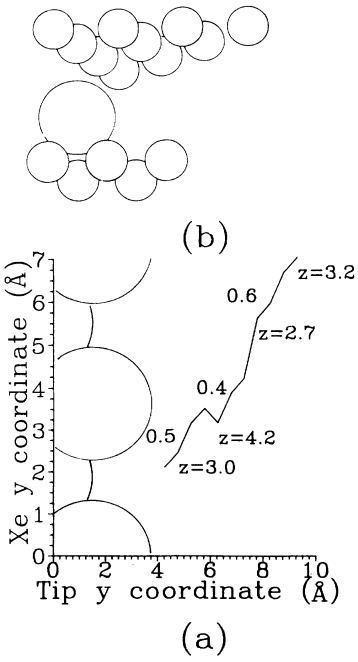

FIG. 7. Same as Fig. 5, but for a tip height of $z_{tip} = 5.6$ Å.

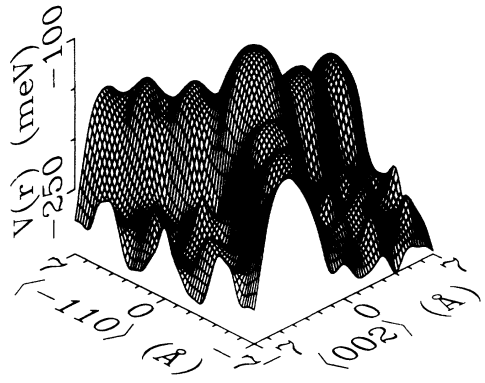

FIG. 8. Potential energy surface when considering only the interaction between a Xe atom and the sharp (111) tip. The Xe atom hardly finds any corrugations when moving away from the tip midpoint, so that it can initially climb up the tip slope.

Å) then, when withdrawing the tip, the noble atom will keep attached to the tip rather than to the surface. This will result in a contaminated tip. For all tip heights, the xenon physisorption height to the nickel surface does not vary drastically while being dragged (typically ranging from 2.6 to 3.0 Å), so contamination should occur at tip heights smaller than approximately 4.0 Å.

The situation discussed previously changes substantially when considering the (111) tip with three atoms at the end. Here, the xenon binding energy to the threefold tip midpoint is 349 meV, at a physisorption height of 1.87 Å (the presence of the nickel surface is not considered now). This high value for the adsorption makes clear that the xenon atom will tend to stick to the tip, remaining fixed in that position during the carriage and, when withdrawing the tip from the surface, the xenon will be pulled away from the nickel. The tip is again contaminated, but this time the potential created by the tip presents a considerable barrier for the xenon to escape from the threefold tip midpoint site (145 meV). Thus, we conclude that if this tip approaches another surface atom, it will be this surface atom which migrates to another surface unit cell, leaving the "contaminated" tip unchanged, so no transport will be present.

A different transport mechanism could be to regard the contaminated tip as a repulsive tool (via the Xe-Xe repulsion), i.e., pushing instead of pulling . However, this is unlikely since the Xe atom, when being pushed, can escape to other surface unit cells located not necessarily along the y direction. On the other hand, the intensity obtained for this case is too low.

As regards the (110) tips, the same arguments can be applied, but now binding energies are considerably smaller than for the (111) case since the structure is less compact. For the sharp-ended tip the situation is analogous to the previous one, the main differences being: (i) A very small range in tip heights for which transport is possible; only up to 4.3 Å and (ii) the y distance increases, this time varying between 2.8 and 3.3 Å. In Fig. 9(a) we plot the xenon y coordinate versus the tip position for a tip height of 4 Å. Again, intensities are shown to the left of some data points, the corresponding values being within the experimental range. Figure 9(b) shows the corresponding geometry.

Contamination will now be less probable, as the binding energies in the tip slopes are smaller than for the sharp (111) tip by about 50 meV. However, for a very small tip height (less than 3.0 Å), the y distance increases, so that the xenon atom might physisorb at a third or fourth layer of the tip, where the binding energies exceed 260 meV, but these tip heights, on the other hand, yield too high tunneling currents.

Finally, for the tip within a four-atom base [flat (110)], two different situations can be considered. First, if the tip is initially placed right on top of the xenon, the tip height cannot become smaller than 5.9 Å as the minimized potential gives positive energies. The transport is then only possible for a very small range in the tip heights; namely, from 5.9 to 6.3 Å, but then tunneling currents an order of magnitude too small are obtained. Second, we consider lowering the tip further. In this case, we expect the Xe

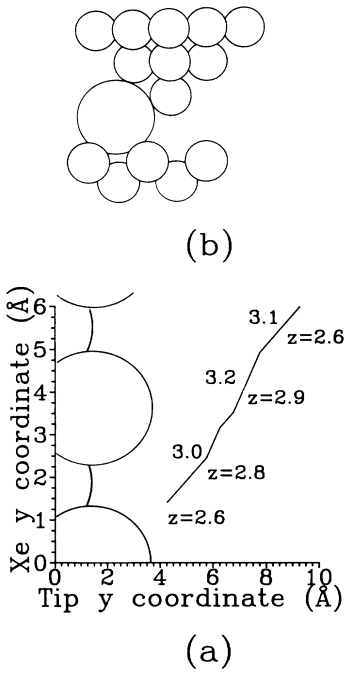

FIG. 9. Description of the transport for the sharp (110) tip at a tip height of $z_{tip} = 4.0$ Å. (a) Xe [002] coordinate (Å) vs tip [002] coordinate (Å), and (b) geometry of the system when the Xe atom is at the hollow site.

atom to migrate to a nearby surface unit cell, pursuing a more stable minimum. Hence, when displacing the tip, the tip slope rather than the twofold site at the tip base would be the main source of the van der Waals attraction. We have studied this case considering an equivalent situation: the tip midpoint is not initially placed on top of the Xe atom, but with a nonzero y distance, or in other words, the Xe atom is assumed to have migrated to the surface unit cell behind the original one along the y direction (the basis of the transport should nevertheless be rather independent of the initial Xe coordinates). For this case, the Xe transport is done with a y distance of 5.0–5.5 Å. Again the hopping effect is present and the calculated intensities agree with the experimental values for tip heights between 4.2 and 4.8 Å. In Fig. 10 we show the carriage process for this case, considering a tip height of 4.4 Å.

Although not explicitly discussed above, as the tip becomes higher, the attractive van der Waals force on the xenon atom obviously decreases, setting a threshold for the tip height beyond which there is no transport. Table IV summarizes the thresholds in the tip heights for successful transport along both directions, as well as the height below which "contamination," if any, will happen. As expected, thresholds along the [$\bar{1}$10] direction are less restrictive than those for the [002] direction. We also give in Table IV the range in tip heights for which the estimated tunneling currents are within the experimental values used by Eigler and Schweizer. Although values for the flat (111) tip appear in this table, we stress that this tip can hardly be accepted as a reasonable approximation to the experimental one used in the transport.

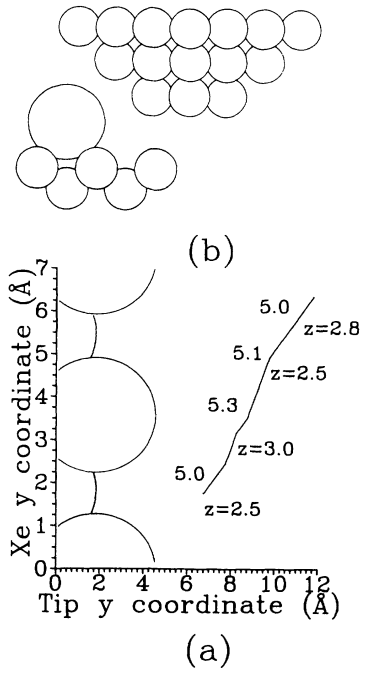

FIG. 10. Description of the transport for the flat (110) tip at a tip height of $z_{tip} = 4.4$ Å. (a) Xe [002] coordinate (Å) vs tip [002] coordinate (Å), and (b) geometry of the system when the Xe atom is at the hollow site.

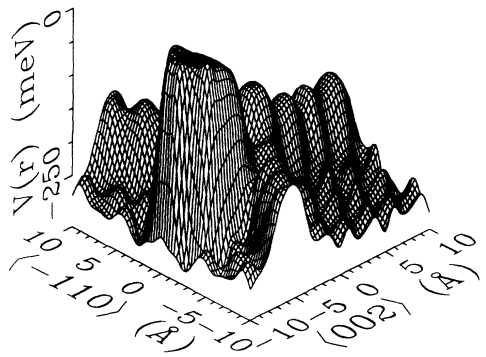

FIG. 11. Potential energy surface when considering the Lennard-Jones interaction between a sharp (111) tip with a Xe atom attached to it and another Xe atom. The minimization with respect to the [110] of the latter was done keeping fixed the tip Xe atom at (−5.4,−0.2,−0.4) Å from the tip midpoint.

As regards the other three tips considered, one finds that the tip heights yielding the correct tunneling current are always below the corresponding thresholds, thus no inconsistency appears between the two theoretical models used here (the fact that these thresholds seem slightly too permissive is probably related to the fitting in the van der Waals asymptotic form).

As the final point in this discussion, we mention the fact that it seems quite plausible that during the transport, the tip height might take values very close to the contamination heights given in Table IV, so we could address the following question: would a contaminated tip still be able to drag another Xe atom? We find that the Xe attached to the tip changes considerably the tip potential profile as seen by another Xe atom in the absence of the Ni surface. This is shown in Fig. 11, where physisorption of a Xe atom at the slope of a sharp (111) tip [with coordinates (−5.4,−0.2,−0.42) Å relative to the tip midpoint] is considered. Now, the tip slope's potential is completely governed by the attached noble atom, which appears as a high protrusion in this energy profile. These severe modifications when compared with the "clean" tip (Fig. 8) are caused by the small Xe-Xe binding energy ($\epsilon_{Xe\text{-}Xe} = 19.2$ meV $= 0.46\epsilon_{Xe\text{-}W}$, while the corresponding separation is large ($\sigma_{Xe\text{-}Xe} = 4.1$ Å $= 1.3\sigma_{Xe\text{-}W}$).[29] Then, when approximating the contaminated tip to another Xe on the surface, the Xe-Xe interaction by itself will not be able to pull the atom away from the fourfold site, but if we make the tip come closer in order to increase the attraction of the W atoms, repulsion between the two Xe atoms will occur. At this point, depending on which one of the two sees a greater corrugation, either the surface Xe will migrate to an adjacent surface unit cell or the Xe on the tip will move further up the slope to another high coordination site.

As seen in Figs. 8 and 11, if we consider migration in the upwards direction, tip corrugations become greater as we move away from its midpoint due to the increase of W nearest-neighbor atoms present, but the initial values give very small potential barriers (if any), certainly smaller than those present at the Ni surface which is 34 meV. Downwards migration can, on the other hand, be readily discarded. Thus, one might expect the Xe at the tip to be pushed upwards along the slope, leaving a re-

TABLE IV. Geometrical limits for transport derived in this work: columns 1 and 2 give the tip height thresholds for both directions, above which the tip will not drag the Xe atom following the Lennard-Jones formalism (accuracy of ±0.1 Å); column 3 shows the ranges in tip heights that yield a tunnel current within the experimental values (accuracy of ±0.1 Å); column 4 gives tip heights below which tip contamination is probable.

Tip	Transport threshold (Å)		Tip height range	Contamination
	[−110]	[002]	for valid I (Å)	height (Å)
(111) Sharp	5.9	5.6	3.9 → 5.0	4.0
(111) Flat	6.3	6.3	4.3 → 5.5	5.5
(110) Sharp	5.3	4.3	3.7 → 4.6	2.5
(110) Flat	6.3	6.1	4.3 → 5.3	4.0

gion at the end of the tip free to transport the Xe surface atom from one surface unit cell to another. Hence, the tip becomes a small "reservoir" for the noble atoms, which can adsorb a certain number of Xe atoms per slope, until one of these reaches a too high potential barrier to continue moving up. Furthermore, when this "reservoir" saturates, no other Xe atoms will be allowed to get attached to the tip when it is withdrawn. Therefore, based on the above simple grounds, one can expect that a "contaminated" STM tip might still position Xe atoms where desired.

V. CONCLUSIONS

We have simulated from a theoretical point of view the Eigler and Schweizer experiment showing the capabilities of a scanning tunneling microscope to transport at will xenon atoms on a Ni(110) surface. In our study, we have stressed the role of two key parameters: the shape of the tip and its distance to the surface. At the same time as the Lennard-Jones analysis was carried out we have calculated tunneling currents for each situation. When comparing with the available experimental results the following conclusions can be drawn.

(1) Of the four tips we have studied only one model can be clearly discarded; the (111) ended on a three-atom platform. First, this tip yields a too broad image for the xenon atom (Fig. 3) and, second, it binds too strongly the xenon at the hollow site preventing any subsequent movement. This is due to the high potential barriers created at this adsorption site.

(2) STM tips must have relatively sharp ends, but never constituting compact high coordination sites, as otherwise the Xe will simply stick to the tip and no transport will occur. This also means that the tip is more likely to be formed by convergent sloped planes than just chemisorbing a metal atom at flat surfaces.

(3) During the transport, the xenon remains 3–5 Å behind the tip midpoint. We interpret this as an indication of the important role played by final atoms sitting on the tip's slopes.

(4) The tunnel current can, then, be achieved directly from the tip to the substrate, not being only mediated by the adsorbed atom.

(5) The most likely distance between the tip and the substrate to achieve the xenon transport ranges from 4.0 to 5.0 Å.

(6) Tips may become contaminated by physisorbing Xe atoms, but still they can contribute to the transport provided that the number of contaminants is not high.

(7) The transport mechanism for the Xe might not look like an object continuously sliding on the surface, but rather, the Xe atom follows a certain hopping process.

ACKNOWLEDGMENTS

We are grateful to Dr. R. Ramirez for many interesting and useful discussions on the subject. This work has been partially financed by the Spanish CICYT under Contracts Nos. MAT89-582 and MAT89-165. F.F. acknowledges help by Iberduero S.A.

[1] D.M. Eigler and E.K. Schweizer, Nature **344**, 524 (1990).
[2] A. Martin-Rodero, F. Flores, and N.H. March, Phys. Rev. B **38**, 10047 (1988).
[3] J. Ferrer, A. Martin-Rodero, and F. Flores, Phys. Rev. B **38**, 10113 (1988).
[4] D.M. Eigler, C.P. Lutz, and W.E. Rudge, Nature **352**, 600 (1991).
[5] I.W. Lyo and P. Avouris, Science **253**, 173 (1991).
[6] H. Fuchs and T. Schimmel, Adv. Mater. **3**, 112 (1991).
[7] R. Gomer, *Field Emission and Field Ionization* (Harvard University Press, Cambridge, Massachusetts, 1961).
[8] L.V. Keldysh, Zh. Eksp. Teor. Fiz. **47**, 1515 (1964) [Sov. Phys. JETP **20**, 1018 (1965)].
[9] C. Caroli, R. Combescot, P. Nozieres, and D. Saint-James, J. Phys. C **5**, 21 (1972).
[10] D.A. Papaconstantopoulos, *Handbook of the Band Structure of Elemental Solids* (Plenum, New York, 1986).
[11] E. Clementi and C. Roetti, At. Data Nucl. Data Tables **14**, 177 (1974).
[12] F. Herman and S. Skillman, *Atomic Structure Calculations* (Prentice Hall, Englewood Cliffs, NJ, 1963).
[13] E.C. Goldberg, A. Martin-Rodero, R. Monreal, and F. Flores, Phys. Rev. B **39**, 5684 (1988).
[14] D.M. Eigler, P.S. Weiss, E.K. Schweizer, and N.D. Lang, Phys. Rev. Lett. **66**, 1189 (1991).
[15] D.R. Hamann, M. Schluter, and C. Chiang, Phys. Rev. Lett. **43**, 1494 (1979).
[16] G. Kerker, J. Phys. C **13**, L189 (1980).
[17] S.G. Louie, S. Froyen, and M.L. Cohen, Phys. Rev. B **26**, 1738 (1982).
[18] *Handbook of Chemistry and Physics*, edited by R.C. Weast and M.J. Astle (CRC, Boca Raton, Florida, 1979).
[19] G. Vidali, G. Ihm, Hye-Young Kim, and M.W. Cole, Surf. Sci. Rep. **12**, 4 (1991).
[20] E. Zaremba and W. Kohn, Phys. Rev. B **13**, 2270 (1976).
[21] N. Ebsferg and J.K. Norskov, Phys. Rev. Lett. **45**, 807 (1980).
[22] J.F. Annett and P.M. Echenique, Phys. Rev. B **34**, 6853 (1986).
[23] G. Vidali and M.W. Cole, Surf. Sci. **110**, 10 (1981).
[24] C. Schwartz and R.J. Le Roy, Surf. Sci. **166**, L141 (1986).
[25] A. Dalgarno, Adv. Chem. Phys. **12**, 143 (1967).
[26] M.J. Dresser, T.E. Madey, and J.T. Yates, Jr., Surf. Sci. **42**, 533 (1974).
[27] R.G. Wilmoth and S.S. Fisher, Surf. Sci. **72**, 693 (1978).
[28] B.E. Nieuwenhuys, O.G. Van Aardenne, and W.M.H. Sachtler, Chem. Phys. **5**, 418 (1974).
[29] S.M. Valone and J.D. Doll, Surf. Sci. **139**, 478 (1984).